BIOCHEMISTRY
including biophysical chemistry & molecular biology
Article

Biochemistry **2010,** *49,* 3611–3618 3611
DOI: 10.1021/bi100070r

Analysis of Imatinib and Sorafenib Binding to p38α Compared with c-Abl and b-Raf Provides Structural Insights for Understanding the Selectivity of Inhibitors Targeting the DFG-Out Form of Protein Kinases‡

Haridasan V. Namboodiri,*,§ Marina Bukhtiyarova,§ Joseph Ramcharan,§ Michael Karpusas,§,⊥ Younghee Lee,∥ and Eric B. Springman§,@

§*Department of Biology and* ∥*Department of Chemistry, Locus Pharmaceuticals, Inc, Four Valley Square, 512 East Township Line Rd, Blue Bell, Pennsylvania 19422.* ⊥*Present address: Laboratory of Physics, Department of Science, Agricultural University of Athens, Iera Odos 75, Athens 11855, Greece.* @*Present address: Celtaxsys, Inc., ATDC Biosciences Center, 311 Ferst Dr., Atlanta, GA 30332.*

Received January 15, 2010; Revised Manuscript Received March 25, 2010

ABSTRACT: Protein kinases c-Abl, b-Raf, and p38α are recognized as important targets for therapeutic intervention. c-Abl and b-Raf are major targets of marketed oncology drugs Imatinib (Gleevec) and Sorafenib (Nexavar), respectively, and BIRB-796 is a p38α inhibitor that reached Phase II clinical trials. A shared feature of these drugs is the fact that they bind to the DFG-out forms of their kinase targets. Although the discovery of this class of kinase inhibitors has increased the level of emphasis on the design of DFG-out inhibitors, the structural determinants for their binding and stabilization of the DFG-out conformation remain unclear. To improve our understanding of these determinants, we determined cocrystal structures of Imatinib and Sorafenib with p38α. We also conducted a detailed analysis of Imatinib and Sorafenib binding to p38α in comparison with BIRB-796, including binding kinetics, binding interactions, the solvent accessible surface area (SASA) of the ligands, and stabilization of key structural elements of the protein upon ligand binding. Our results yield an improved understanding of the structural requirements for stabilizing the DFG-out form and a rationale for understanding the genesis of ligand selectivity among DFG-out inhibitors of protein kinases.

Imatinib (Gleevec, STI-571, Novartis Pharma AG) (Figure 1) is a therapeutic drug that is approved for the treatment of chronic myelogeneous leukemia (CML) and gastrointestinal stromal tumors (GST) (*1*, *2*). Sorafenib (Nexavar, BAY-43006, Bayer Pharma) is a therapeutic agent that is approved for the treatment of advanced renal cell carcinomas (RCC) and nonresectable hepatocellular carcinomas (HCC) (*3*, *4*). Both drugs target protein kinases, and their clinical success has been largely attributed to their ability to bind to an inactive conformation of their targets inside cells (*5*). Binding of these compounds is associated with a conformational change of the Asp-Phe-Gly (DFG)[1] motif and nearby activation loop (A-loop) of the protein kinase to the "DFG-out state" (*6*). In this conformation, the protein is inactive because binding of ATP is sterically excluded by a portion of the DFG motif and the arrangement of the catalytic groups is disrupted. Hence, this mode of action is sometimes termed "allosteric inhibition", and the inhibitors are often termed "allosteric inhibitors".

Imatinib is a phenylaminopyrimidine compound that binds to the nonphosphorylated c-Abl kinase domain. Imatinib has also been shown to inhibit c-Kit and PDGR kinases (*7*) but not known to bind or inhibit p38α kinase. X-ray crystallography has revealed that Imatinib binds to c-Abl in an inactive DFG-out conformation that is not compatible with substrate binding (*5*). In this binding mode, Imatinib adopts an extended configuration. Interestingly, it was also shown that Imatinib binds to the highly homologous c-Src kinase in the same conformation as to c-Abl (*8*), even though Imatinib was previously reported to be markedly less inhibitory toward c-Src kinase activity (IC_{50} > 100 μM, compared to 0.025−0.2 μM for c-Abl) (*9*). In another crystal structure, it was shown that Imatinib binds to Syk kinase in a different conformation of both protein and compound (*10*). In this binding mode, the ligand undergoes a rotation around the phenylamino linker between the pyrimidine and the phenyl ring to form a "folded" configuration of the compound that then binds to the DFG-in form of Syk. Since Imatinib has a significantly different affinity for these two kinases (K_D > 10 μM for Syk compared to 0.012 μM against c-Abl) (*11*), it was proposed that the preferred conformation of Imatinib with phosphorylated c-Abl (against which it is less active) may be the same cis conformation (*10*).

Sorafenib is a biaryl urea compound that targets all three members of the Raf family of protein kinases (a-Raf, b-Raf, and c-Raf), as well as PDGFR, VEGF 2/3, and c-Kit kinases (*12*). In a situation similar to the mode of binding of Imatinib to c-Abl kinase, Sorafenib binds to b-Raf and p38α in the DFG-out conformation (*6*, *13*).

‡The atomic coordinates and structure factors of p38α in complex with Imatinib and Sorafenib have been deposited with the Protein Data Bank as entries 3HEC and 3HEG, respectively.

*To whom correspondence should be addressed. E-mail: vnamboodiri@ansarisbio.com. Phone: (215) 358-2012. Fax: (215) 358-2030.

[1]Abbreviations: MAPK, mitogen-activated protein kinase; DFG, Asp-Phe-Gly in the activation loop; A-loop, activation loop; P-loop, Gly-rich loop; SASA, solvent accessible surface area; SPR, surface plasmon resonance; rmsd, root-mean-square deviation.

Published on Web 03/25/2010

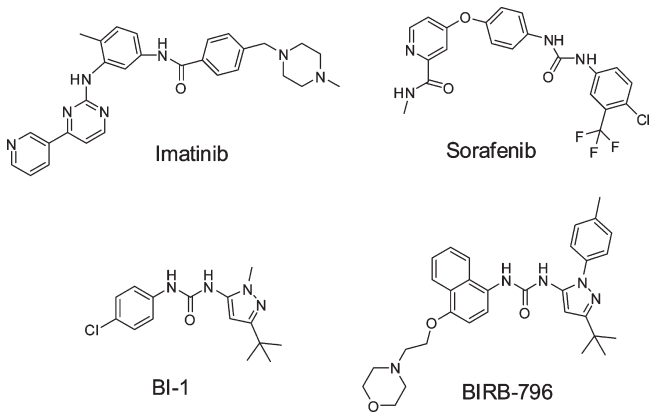

FIGURE 1: Chemical structures of Imatinib, Sorafenib, BI-1, and BIRB-796.

Table 1: Crystallographic Diffraction and Refinement Statistics for p38α with Imatinib and Sorafenib

	p38α−Imatinib	p38α−Sorafenib
resolution (Å)	2.5	2.2
space group	$P2_12_12_1$	$P2_12_12_1$
unit cell dimensions	a = 65.0 Å, b = 74.0 Å, c = 74.5 Å, α = 90°, β = 90°, γ = 90°	a = 65.5 Å, b = 74.2 Å, c = 77.8 Å, α = 90°, β = 90°, γ = 90°
total no. of reflections	437317	205067
no. of unique reflections	14641	19920
overall completeness (last shell) (%)	99.9 (100.0)	99.6 (99.8)
R_{merge} (last shell) (%)	7.7 (39.7)	8.6 (55.9)
$I/\sigma(I)$ (last shell)	20.3 (3.9)	20.2 (2.1)
R_{work} (%)	21.8	23.6
R_{free} (%)	29.8	30.9
rmsd for covalent bond lengths (Å)	0.018	0.0016
rmsd for bond angles (deg)	1.91	1.71
average protein chain B factor (Å^2)	38.98	42.16
average solvent B factor (Å^2)	38.68	41.87
average B factor, other atoms (Å^2)	48.11	30.99
average B factor, all atoms (Å^2)	39.16	42.02

p38α is one of four p38 isotypes that belong to the mitogen-activated protein kinase (MAPK) family of Ser/Thr protein kinases, which together with the extracellular signal-regulated kinase (ERK) and c-Jun N-terminal kinase (JNK) integrates and processes various extracellular signals (*14*). It is one of the most studied members of the p38 MAP kinase family and has been characterized in great detail. Upon activation, it is doubly phosphorylated at residues Thr180 and Tyr182 in a TGY sequence in the activation loop (*15*). Although there are approximately 90 crystal structures of the nonphosphorylated form of p38α deposited in the Protein Data Bank (PDB), a crystal structure of the dually phosphorylated form of p38α is not reported. However, the structure of the phosphorylated p38γ isoform has been determined in complex with an ATP analogue (PDB entry 1CM8) (*16*).

A number of p38α inhibitors have progressed into clinical trials for treatment of a variety of inflammatory diseases (*17*). Most of these compounds bind to the DFG-in form of the protein and are directly ATP competitive (*18*, *19*). Members of another class of inhibitors, exemplified by BIRB-796 and BI-1, bind to a cryptic site adjacent to the ATP binding site (*20*, *21*). BI-1 is an *N*-pyrazole-*N*-aryl urea inhibitor of p38α with modest activity which was subsequently refined to BIRB-796 as a potent p38α inhibitor. The binding of this class of compounds requires a conformational change of the activation loop to the DFG-out state, similar to that observed for Imatinib in c-Abl and Sorafenib in b-Raf. Both BI-1 and BIRB-796 were shown to have unique binding properties characterized by slow on rates (k_{on}) and long off rates (k_{off}) (*20*). The slow binding was explained by the rate-determining requirement for a conformational change in the DFG motif. BIRB-796 was shown to be a potent inhibitor of LPS-stimulated TNFα production in vitro and in vivo and subsequently entered the clinic but was later discontinued (*21*).

Imatinib has been reported to be noninhibitory toward non-activated p38α ($K_D \geq 10\ \mu$M) (*11*), suggesting that the inhibitor either does not bind to the protein or binds in a folded conformation as seen with Syk (*10*). Sorafenib, on the other hand, has been shown to inhibit p38α (Table 1). Here, we report a novel X-ray crystal structure of p38α in complex with Imatinib. We also determined the cocrystal structure of p38a with Sorafenib in a ligand conformation very distinct from a recently reported structure (*13*). We compared our structures to published structures of Imatinib in complex with c-Abl, c-Kit, Lck, and c-Src and Sorafenib in complex with b-Raf to analyze differences in key binding interactions, changes in buried solvent accessible surface area (SASA) of the ligands, and stabilization of key structural elements of the protein upon ligand binding. We also conducted a functional analysis using surface plasmon resonance (SPR) to determine the binding kinetics of Imatinib, Sorafenib, and BI-1 to p38α kinase. Our results provide a basis for rationalizing the properties of binding of compounds to p38α and insights into

structural requirements for the design of selective protein kinase inhibitors targeting the DFG-out state.

MATERIALS AND METHODS

Protein Expression and Purification. The wild-type p38α protein was expressed in *Escherichia coli* as described previously (*22*). For purification, the cell pellet was resuspended in a lysis buffer containing 50 mM Tris (pH 7.4), 500 mM NaCl, and 10 mM imidazole and lysed using an EmulsiFlex-C5 homogenizer (Avestin). The supernatant was applied to a Metal Chelate Ni^{2+} XK 16 column (GE Healthcare, Piscataway, NJ), previously equilibrated with lysis buffer. Bound protein was eluted with an imidazole gradient, and the p38α-containing fractions were combined and dialyzed overnight at 4 °C against 50 mM Tris (pH 7.4), 100 mM NaCl, and 1 mM DTT. A Mono Q HR 10/10 column equilibrated in 50 mM Tris (pH 7.4), 50 mM NaCl, 5% glycerol, 10 mM $MgCl_2$, and 1 mM DTT was used subsequently to further purify the protein to homogeneity. Bound protein was eluted with a linear NaCl gradient, and the pure fractions were pooled and concentrated to ~16 mg/mL, divided into aliquots, flash-frozen in liquid nitrogen, and stored at −80 °C.

Protein Kinase Assay. The protein kinase activity of dually phosphorylated p38α (Invitrogen, catalog number PV3304) was determined by measuring the incorporation of ^{33}P from [γ-^{33}P]ATP into the GST-ATF2 substrate as described previously (*22*). The reactions were conducted in a final volume of 50 μL of assay buffer containing 2.5 Ci of [γ-^{33}P]ATP, 10 μM cold ATP, and 2 μM GST-ATF2. The ligands were preincubated with p38α for 20 min at 30 °C, after which the reactions were initiated by the addition of GST-ATF2 and ATP. Samples were incubated for 70 min at 30 °C before the reaction was stopped. The phosphorylated substrate was captured on a phosphocellulose 96-well plate (Millipore MAPHNOB 10) and counted in a Beckmen-Coulter LS6500 liquid scintillation counter. IC_{50} was defined as the concentration of the test compound that caused a 50% decrease in the maximal level of inhibition of p38α activity and was calculated from replicate curves using GraphPad Prism.

SPR Biacore Binding Kinetics. Inhibitor binding kinetics was determined using a BIAcore method as previously described (*23*). Unphosphorylated p38α was immobilized to the surface of the CM5 sensor chip by standard amine coupling via exposed primary amines on the proteins in the presence of saturating concentrations of SB-203580 (10 μM) or BI-1 (500 μM). Immobilization reactions were conducted at 25 °C in HBS-EP buffer at a flow rate of 10 μL/min. Flow cells were activated for 7 min via injection of 70 μL of a 1:1 mixture of 50 mM NHS and 200 mM EDC. A 50 μg/mL solution of p38α protein (50 μL) was mixed with 10 μM SB-203580 in sodium acetate (pH 5.5) and injected for 5 min. Subsequently, 35 μL of ethanolamine was injected to block any remaining activated ester groups. SB-203580 was readily removed from the immobilized p38α during the postcoupling blocking and washing steps. Typical immobilization levels ranged from 3000 to 6000 resonance units (RU). Flow cells treated in the absence of p38α protein served as reference surfaces.

Kinetic Biosensor Data Analysis. All biosensor kinetic data were processed using SCRUBBER (BioLogic Software Pty Ltd.) before kinetic analysis according to the manufacturer's instructions. In brief, the data were referenced by subtracting an unmodified surface so that the binding responses collected over the active surfaces were corrected for bulk refractive index changes. Next, the association phase data were solvent corrected to account for any signal fluctuation throughout the experiment due to subtle DMSO concentration differences. Finally, the response from an average of the blank injections was subtracted to exclude any differences between the active and reference flow cells resulting from systematic artifacts.

Determination of Crystal Structures. The p38α ligand complexes were prepared by incubation of the pure protein with the ligand at a molar ratio of 1:5 for ~1 h on ice (*24*). Sitting drops were set up by mixing the complex with a reservoir solution containing 10−20% PEG 4000, 0.1 M cacodylic acid (pH 6.0), and 50 mM *n*-octyl β-D-glucoside at 20 °C. Crystals could be obtained only by seeding with previously grown cocrystals of p38α. Imatinib cocrystals appeared after ~2 weeks, while Sorafenib cocrystals appeared in ~2 days. To determine the structure of the p38α−Imatinib complex, we screened a large number of cocrystals for X-ray diffraction. Of six data sets we collected, electron density for the bound inhibitor was visible in only one determined structure. In contrast, of three data sets we collected for the p38α−Sorafenib complex, we could see unambiguous electron density for the bound inhibitor in all three structures. Overall, the p38α−Sorafenib cocrystals were easier to grow and diffracted better in comparison to the p38α−Imatinib cocrystals. The crystals were cryoprotected in a solution containing the mother liquor and 25% ethylene glycol. X-ray diffraction data were collected at 100 K, using an ADSC Quantum 4 CCD detector at the X4A beamline of the National Synchrotron Light Source (Brookhaven National Laboratory, Upton, NY). The data were processed using HKL (*25*). Both structures were determined by Molrep (*26*) using PDB entry 1ZYJ as the starting model. REFMAC (*27*) was used for refinement and COOT (*28*) for model building. Figures were generated using Pymol (DeLano Scientific).

RESULTS

X-ray Crystal Structures. Imatinib binds to p38α in the interdomain cleft extending from the ATP binding site into the allosteric pocket in a conformation similar to its bound form in c-Abl, c-Kit, and c-Src kinases (*5*, *8*, *30*) (Figure 2B). In the ATP binding site, Imatinib interacts with p38α via two hydrogen bonds to the hinge (Figure 4A), the first through the pyrimidine N and the backbone amino nitrogen of Met109 and the second through the NH linker and Oγ-1 hydroxyl of Thr106. The amide nitrogen and oxygen of the inhibitor form a hydrogen bond to the δ-carboxylate oxygen of Glu71 and amino nitrogen of Asp168, respectively. The piperazine group extends into the solvent but is still within the protein cavity. The nitrogen of the piperazine ring is positioned over two main chain carbonyl oxygens of Ile147 and His148. In solution, the piperazine nitrogen may be protonated and form a hydrogen bond to the carbonyl oxygens. A central water molecule coordinates among the pyrimidine nitrogen of the inhibitor, the ε-nitrogen of Lys53, and the Asp168 main chain carbonyl oxygen. The central aryl ring occupies the allosteric pocket created by the displacement of Phe169 of the DFG motif. The activation loop beyond Gly170 and the P-loop were disordered in the electron density maps and therefore could not be modeled.

Sorafenib binds to p38α in the DFG-out form with a ligand conformation different from that reported by Simard et al. (PDB entry 3GCS) (*13*). In our crystal structure, the pyridine nitrogen and the ethyl picolinamide moiety in the hinge are within hydrogen bonding distance of the Met109 main chain (Figures 3B and 4B). In PDB entry 3GCS, however, the trajectory of the *N*-methyl-4-phenoxypicolinamide group is different. The pyridyl

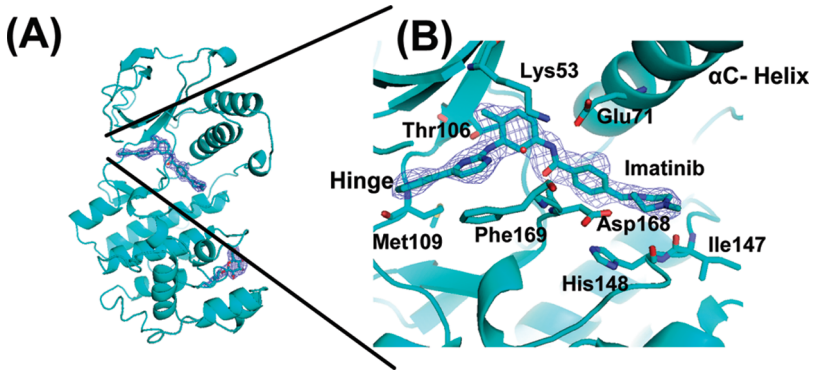

FIGURE 2: Crystal structure of the p38α−Imatinib complex. (A) Overall fold of p38α kinase in complex with Imatinib. The electron density map ($2F_o - F_c$) contoured at 1σ is shown as blue mesh for Imatinib and the detergent (β-octyl glucoside). (B) Inhibitor binding site showing interactions of p38α with Imatinib.

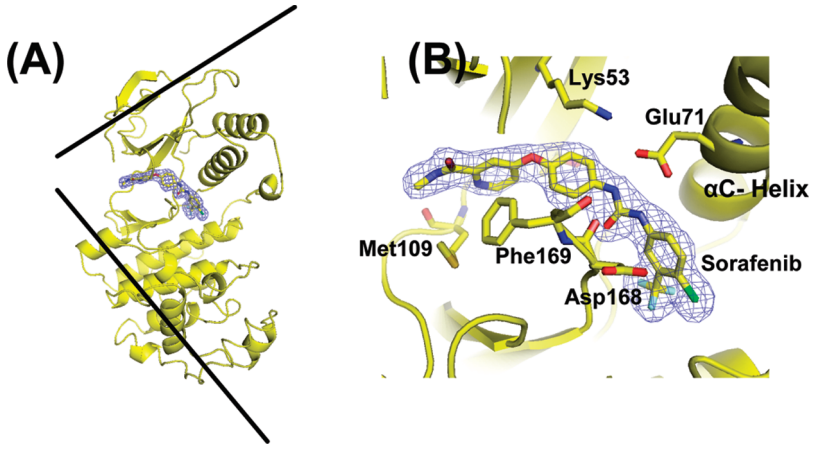

FIGURE 3: Crystal structure of p38α in complex with Sorafenib. (A) Overall fold of p38α kinase in complex with Sorafenib. The electron density map ($2F_o - F_c$) contoured at 1σ is shown as blue mesh for Sorafenib. (B) Inhibitor binding site showing interactions of p38α with Sorafenib.

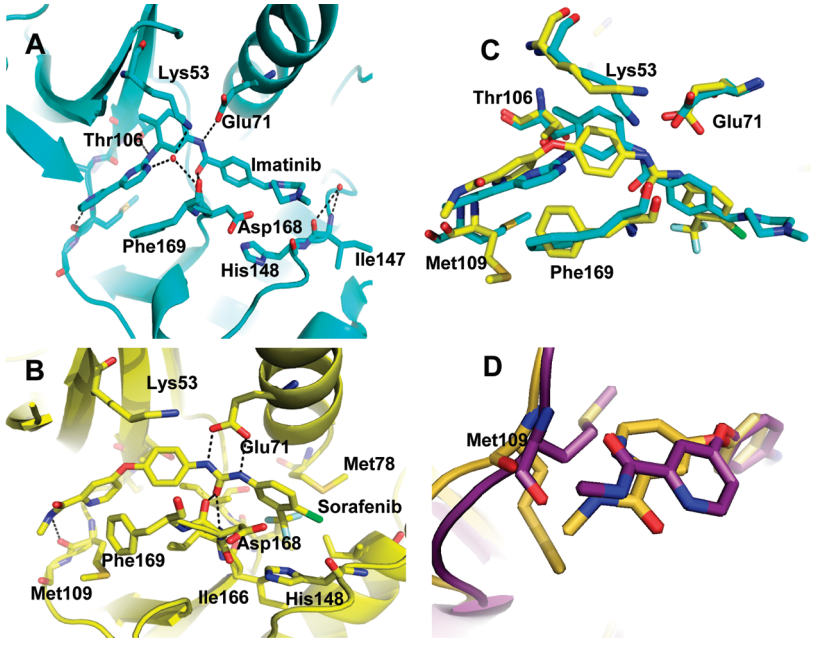

FIGURE 4: Comparison of p38α complexes with Imatinib and Sorafenib. (A) Close-up showing the Imatinib binding mode within p38α and H-bond interactions. (B) Close-up showing the Sorafenib binding mode within p38α and H-bond interactions. (C) Superposition of both structures showing the differences in the orientation of critical residues in the binding site. The Imatinib structure is colored cyan and Sorafenib yellow. (D) Superposition of the p38α−Sorafneib complex determined by Simard et al. and our p38α−Sorafenib structure showing the difference in the conformation of the terminal group near the hinge.

nitrogen in the published structure is rotated and does not interact with the hinge. Instead, the carbonyl moeity of the picolinamide is within hydrogen bonding distance of Met109 (Figure 4D). The Met109 side chain is also rotated out of the inhibitor binding site in PDB entry 3GCS when compared to our structure. The binding mode of Sorafenib seen in our crystal structure is more similar to its bound form with b-Raf (PDB entry 1UWH) than with PDB entry 3GCS. All analysis of the p38α−Sorafenib structure discussed in this paper refers to our crystal structure.

Kinase Assay. The ability of Imatinib, Sorafenib, and BI-1 to inhibit p38α activity in vitro was analyzed in an enzymatic [^{33}P]ATP kinase assay using ATF2 as the protein substrate. The IC_{50} values for the three inhibitors span a 1000-fold range, with Sorafenib being the most potent inhibitor among the three with an IC_{50} of 0.057 μM (Table 2). BI-1 exhibited a significantly lower potency (IC_{50} = 1.8 μM), and Imatinib was found to be weakly inhibitory with an IC_{50} of 70 μM.

SPR Biacore Binding Affinity Studies. Using SPR, we determined the association rate constant (k_a), the dissociation rate constant (k_d), and the equilibrium binding constant (K_D) of Imatinib, Sorafenib, BIRB-796, and BI-1 with p38α (Table 2). Imatinib had an on rate of 1.1×10^4 M^{-1} s^{-1} and off rate of 0.38 s^{-1}, resulting in an overall lower binding affinity of 34 μM. Sorafenib, on the other hand, had an on rate of 9.5×10^4 M^{-1} s^{-1} and an off rate of 0.018 s^{-1}, resulting in a binding constant of 0.18 μM. BI-1 had an on rate of 5.8×10^4 M^{-1} s^{-1}, an off rate of 0.062 s^{-1}, and a binding affinity of 1.1 μM. BIRB-796 had an on rate of 8.5×10^4 M^{-1} s^{-1} and an off rate of 8.3×10^{-6} s^{-1} which translated into a binding affinity of 0.001 μM. All four inhibitors exhibited association rate constants (k_a) within the same order of magnitude. Dissociation rate constants (k_d), however, varied by several orders of magnitude, with BI-1, Sorafenib, and BIRB-796 showing progressively slower off rates reflecting the higher stability of these complexes. In contrast, Imatinib binding is characterized by an off rate that is 20 times faster than that of Sorafenib, reflecting the poor stability of its complex with p38α.

Solvent Accessible Surface Area of Ligands. We generated protein ligand interaction diagrams using MOE (Chemical Computing Group) (*31*) to determine the extent of the ligands that are exposed to solvent in their respective structures. We found that the two terminal groups in Imatinib (pyridine group near the hinge and methylpiperazine group near the HRD loop) and Sorafenib (ethylpicolinamide near the hinge and the chlorophenyl group near the HRD loop) are exposed to solvent to different extents in each of the structures (data not shown). In the case of Imatinib, the methylpiperazine group is solvent-exposed to a similar extent in p38α, c-Abl, c-Kit, Lck, and c-Src (data not shown). However, the extent to which the terminal pyrimidopyridine group follows the order c-Abl < c-Kit < Lck < p38α < c-Src from least solvent exposed to highest solvent exposed. In the case of Sorafenib, the terminal methyl group attached to the picolinamide moiety is more exposed in p38α than in b-Raf.

Using another script in MOE, we calculated SASA for the bound ligands when they bind to their respective proteins, and the results are listed in Table 3. Imatinib in the c-Abl and c-Kit protein structures has only 35.4 and 41.2 Å^2 of its surface area exposed, respectively, the rest being buried inside the protein structure. Imatinib, which is moderately active against Lck, has a SASA value of 65.0 Å^2. Interestingly, in p38α (SASA = 89.6 Å^2) and c-Src (SASA = 190.0 Å^2), the values were substantially higher. In the Sorafenib complexes, the SASA values for all three structures were remarkably similar [44.8 Å^2 for p38α, 49.9 Å^2 for b-Raf, and 49.2 Å^2 for the b-Raf mutant (Table 3)]. BIRB-796 had a SASA value of 40.4 Å^2, while BI-1 had a lower value of 25.8 Å^2.

Buried Surface Area of Hydrophobic Residues upon Ligand Binding. To investigate how binding of Imatinib, Sorafenib, BI-1, and BIRB-796 affects the arrangement of hydrophobic residues in the protein upon binding, we calculated the percentage of all the hydrophobic protein residues lining the inhibitor binding site that becomes exposed to solvent after ligand binding. In the Imatinib structures, of the 13 hydrophobic residues, three residues markedly differ in their extent of solvent exposure in p38α when compared with c-Abl (Figure 5A). The first residue is the equivalent Phe169 of p38α. It becomes more exposed (22% buried) in p38α in comparison to c-Abl (Phe382) and c-Kit (Phe811) where it is completely buried. In Lck (Phe405) and c-Src (Phe383), the residues are exposed to similar extents (78% buried). The second residue is the equivalent Leu108 in p38α. It is 32% buried in p38α in contrast to 72% in c-Abl (Phe317). In c-Kit, Lck, and c-Src, the equivalent residue is polar and is replaced with a tyrosine. The equivalent Val30 of p38α of the P-loop is the third residue that is exposed to different extents. In p38α, it is 42% buried compared to ~80% in c-Abl (Leu248) and c-Kit (Leu595). In c-Src, however, Leu273 is the most exposed (24% buried).

Table 2: Summary of Enzymatic IC_{50} Values, Kinetic Rates, and Dissociation Constants Determined by Surface Plasmon Resonance (Biacore) for Inhibitors Binding to p38α Kinase

compound	IC_{50} (μM)	K_d (s^{-1})	K_a (M^{-1} s^{-1})	K_D (μM)
BIRB-796	0.018	8.3×10^{-6}	8.5×10^4	0.001
Sorafenib	0.057	0.018	9.5×10^4	0.18
BI-1	1.8	0.062	5.8×10^4	1.1
Imatinib	70.0	0.38	1.1×10^4	34.0

Table 3: Calculated Solvent Accessible Surface Areas of Different Ligands in Their Protein Structures[a]

Imatinib complexes			Sorafenib complexes			p38α complexes		
	IC_{50} (μM)	SASA (Å^2)		IC_{50} (μM)	SASA (Å^2)		IC_{50} (μM)	SASA (Å^2)
c-Abl (1IEP)	0.10	35.4	p38α	0.057	44.8	BI-1 (1KV1)	1.80	25.8
c-Kit (1T46)	0.40	41.2	b-Raf (1UWH)	0.40	49.9	BIRB-796 (1KV2)	0.018	40.4
LcK (2PLO)	1.0	65.0	b-Raf-V600E (1UWJ)	1.0	49.2	Sorafenib	0.057	44.8
p38α	70.0	89.4				Imatinib	70.0	89.4
c-Src (2OIQ)	100.0	191.0				Pyk2 (3FZS)	1.5	115.1

[a]Inhibitors with lower SASA values appear in the first three rows, and inhibitors with higher SASA values appear in the last two rows.

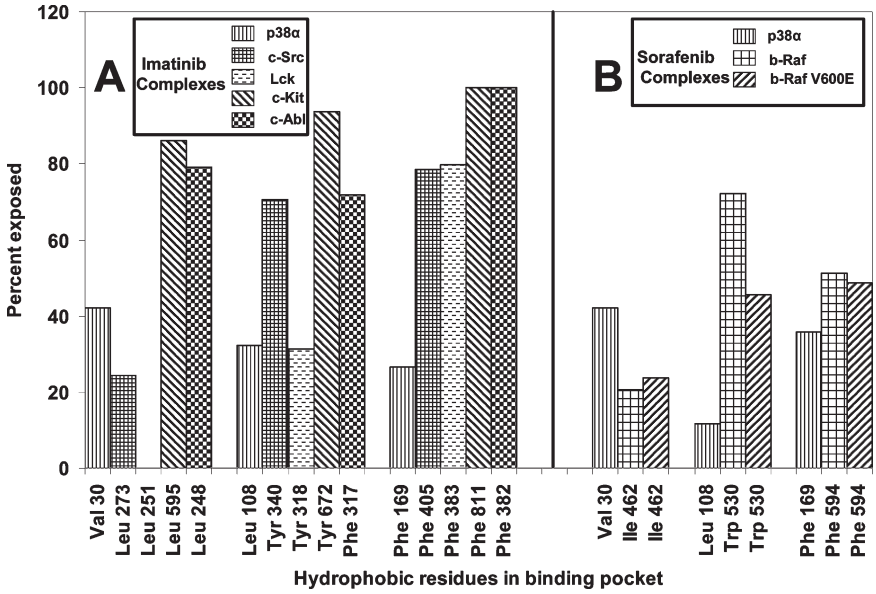

FIGURE 5: Extent of exposed hydrophobic residues within the ligand binding site of Imatinib- and Sorafenib-bound structures. (A) The percentage of hydrophobic protein residues within the Imatinib binding pocket that become exposed upon ligand binding was calculated using a script in MOE (Chemical Computing Group). Of the 13 hydrophobic residues in the binding site, three residues that differ significantly in terms of the extent of solvent exposure are shown. The residues are part of the P-loop, hinge, and DFG loop, respectively. (B) Extent of exposed hydrophobic residues within the ligand binding site of Sorafenib-bound structures. There are 12 hydrophobic residues comprising the ligand binding site in the Sorafenib structures. The hinge residue (equivalent to Leu108 in p38α) is not part of the ligand binding site in these complexes. The closest residue to the hinge (Leu104) is shown instead. There is not much difference in the extent of the three hydrophobic residues from the P-loop and DFG loop, resulting in comparable binding affinities.

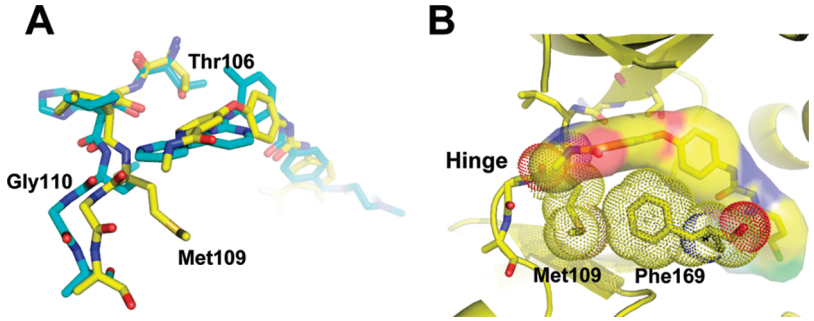

FIGURE 6: Conformational adjustments of the hinge region of p38α in the presence of Imatinib (cyan) and Sorafenib (yellow) structures. (A) Superposition of both crystal structures showing movement of the hinge (~1.9 Å) in the Sorafenib structure. For the sake of clarity, only the hinge residues from Thr106 to Gly110 and the inhibitors are shown. (B) Rotation about the peptide bond between Leu108 and Met109 results in the side chain of Met109 facing the ATP binding site. As a result, Met109 forms a favorable van der Waals interaction with the Phe169 side chain. Sorafenib is shown as a transparent surface, and the side chains of Met109 and Phe169 are shown as dotted surfaces.

In the Sorafenib structures, the extent to which the three equivalent hydrophobic residues discussed above are exposed upon ligand binding is not significantly different (Figure 5B). The equivalent residues (Phe169) in p38α and in both b-Raf structures (Phe594) are similarly exposed (~35% buried). The equivalent residue (Leu108) from the hinge in p38α is exposed to a much larger extent than Trp530 in b-Raf. In contrast, the equivalent Val30 in p38α is less exposed than Ile462 of b-Raf.

DISCUSSION

We determined the crystal structures of p38α in complex with Imatinib, as well as with Sorafenib, albeit with a different conformation of the bound inhibitor as reported by Simard et al. (*13*). A comparison of the two crystal structures reported in this paper showed several significant differences in the inhibitor binding site. First, the conformation of the carboxylate side chain of Glu71 is bidentate in the p38α−Sorafenib structure in contrast to the unidentate conformation in the p38α−Imatinib structure (Figure 4C). Although the effect of the different conformation of Glu71 is not clear, it is possible that the bidentate carboxylate oxygens form hydrogen bonds to both urea nitrogens of Sorafenib. Second, in the p38α−Sorafenib complex, the hinge moves ~1.9 Å toward the binding site (Figure 6A). This might be due to the presence of a glycine residue (Gly110), which imparts extra flexibility to the hinge. Third, the peptide bond between Leu108 and Met109 rotates so that the methionine side chain forms a van der Waals interaction with Phe169 (Figure 6B). Fourth, the conformation of the "gatekeeper" residue Thr106 is different. In the p38α−Imatinib structure, the hydroxyl group of Thr106 forms a hydrogen bond with the amino linker between the phenyl and pyrimidine ring. However, in the Sorafenib structure, the side chain conformation of Thr106 undergoes a 180° rotation to face away from the pocket. Lastly, the Phe169 side chain is rotated by ~90° in both structures, resulting in different extents of aromatic interactions with the pyridine ring of Sorafenib or the pyrimidine ring of Imatinib. The conformation of Phe169 is such that its side

chain has a favorable edge-to-face interaction with Sorafenib, while in the Imatinib structure, the interaction with the pyrimidine ring of Imatinib is of a face-to-face nature (Figure 4C). In general, an edge-to-face aromatic interaction is energetically more favorable than a face-to-face aromatic interaction (*32*).

It is generally believed that ligand binding affinity is driven by a combination of polar interactions and hydrophobic contacts contributing ultimately to the overall stability of the complex in solution. While polar interactions are mediated through highly specific interactions such as hydrogen bonds and salt bridges, hydrophobic interactions are largely dependent on the surface area of contact between the ligand and the protein. To improve our understanding of the differences in the binding affinity of the inhibitors in spite of their similar binding modes versus different protein targets, we determined the extent to which the inhibitor is buried within the protein cavity by (a) determining the extent of the inhibitor exposed to solvent, (b) calculating the solvent accessible surface area (SASA) of the ligand, and (c) calculating the percentage of hydrophobic protein residues within the binding pocket that become exposed upon ligand binding.

The SASA values computed for Imatinib were found to be 35.4 and 41.2 Å^2 for c-Abl and c-Kit, respectively, indicating that majority of the inhibitor is bound within the protein and has therefore more surface area to interact with the protein and hence a higher affinity. The higher SASA values for p38α (89.6 Å^2) and c-Src (190.0 Å^2) indicate smaller surface areas for interaction with the protein which correlates with their lower binding affinities (Table 3). Imatinib which is moderately active against Lck had an intermediate SASA value of 65.0 Å^2 and fell between the c-Abl/c-Kit and p38α/c-Src pairs. In the Sorafenib structures, there are no significant differences in SASA values of the ligand between p38α and b-Raf (Table 3). Even though the SASA for BI-1 was smaller than that for BIRB-796, the latter was more potent in p38α inhibition. This can be explained by the fact that BI-1 does not have the hinge interaction, and since it is smaller in comparison to BIRB-796, the SASA per atom for BI-1 could be much higher than for BIRB-796. A recent structure of BIRB-796 with the Pyk2 kinase domain shows that it binds to the DFG-out form of Pyk2 kinase (PDB entry 3FZS) (*29*). BIRB-796 has an IC_{50} of 1.5 μM against Pyk2 and is therefore ~100-fold less active than in p38α. The SASA for BIRB-796 in the Pyk2 protein structure is significantly larger (115.1 Å^2). Overall, we have observed that SASA values for the ligands tend to be lower in protein complexes in which the ligands show more affinity and higher in protein complexes in which they show lower affinity. It can be used as an additional parameter to explain binding affinities toward different protein targets.

In the ligand-free form, kinases adopt a DFG-in conformation in which the phenylalanine residue is buried and is not solvent accessible. The conformational change induced by allosteric inhibitors exposes the phenylalanine residue to the solvent, which is energetically unfavorable, resulting in a reduction in the stability of the protein complex and ligand binding affinity. Part of this energy loss is compensated by a gain in energy due to ligand binding (*22*). The binding of Imatinib, Sorafenib, BI-1, and BIRB-796 to p38α kinase was studied using surface plasmon resonance. Comparison of kinetic parameters for Imatinib and Sorafenib shows that the 200-fold difference in K_D between Imatinib and Sorafenib is derived largely from the faster dissociation rate for Imatinib (~20-fold) and to lesser extent from the more rapid association rate for Sorafenib (~8-fold). These results indicate that Sorafenib has the lowest energy barrier for binding to p38α and forms the most stable complex. Conversely, Imatinib has both the highest energy barrier and lowest complex stability.

The catalytic domains of protein kinases are highly conserved across the kinome (*33*). Therefore, the design of potent kinase inhibitors with a high degree of selectivity continues to be a major challenge for the pharmaceutical industry (*34*). A particular class of inhibitor may often bind in a similar mode to different kinases, and therefore, the basis for selectivity may not be obvious from the analysis of only the bound structures. In this report, we have shown that the mode of binding of Imatinib and Sorafenib in p38α is similar to those of their respective kinase targets (c-Abl and b-Raf) (*5*, *6*). We have also shown that the kinetics of binding of Imatinib to p38α are largely determined by a faster off rate which distinguishes its binding kinetics from those of Sorafenib, BI-1, and BIRB-796. Structural analysis of the protein inhibitor complexes suggests that lower SASA values for ligands correlate with higher binding affinities and higher SASA values with lower binding affinities. Together, the findings in this report provide a better structural understanding of allosteric inhibitors targeting the DFG-out form of protein kinases and a basis for understanding ligand selectivity in protein kinases.

REFERENCES

1. Capdeville, R., Buchdunger, E., Zimmermann, J., and Matter, A. (2002) Glivec (STI571, imatinib), a rationally developed targeted anticancer drug. *Nat. Rev. Drug Discovery 1*, 493–502.
2. Nagar, B., Hantschel, O., Young, M. A., Scheffzek, K., Veach, D., Bornmann, W., Clarkson, B., Superti-Furga, G., and Kuriyan, J. (2003) Structural basis for the autoinhibition of c-Abl tyrosine kinase. *Cell 112*, 859–871.
3. Liu, L., et al. (2005) Sorafenib (BAY 43-9006) inhibits the Raf/MEK/ERK pathway in hepatocellular carcinoma (HCC) cells and produces robust efficacy against PLC/PRF/5 HCC tumors in mice. Poster presentation at the American Association of Cancer Research, National Cancer Institute, European Organization of Research and Treatment of Cancer, Philadelphia.
4. Escudier, B., Szczylik, C., Eisen, T., Oudard, S., Stadler, W., Schwartz, B., Shan, M., and Bukowski, R. (2005) Randomized phase III trial of the multi-kinase inhibitor sorafenib (BAY 43-9006) in patients with advanced renal cell carcinoma (RCC). *Eur. Urol. Suppl. 5*, 287.
5. Nagar, B., Bornmann, W. G., Pellicena, P., Schindler, T., Veach, D. R., Miller, W. T., Clarkson, B., and Kuriyan, J. (2002) Crystal structures of the kinase domain of c-Abl in complex with the small molecule inhibitors PD173955 and imatinib (STI-571). *Cancer Res. 62*, 4236–4243.
6. Wan, P. T., Garnett, M. J., Roe, M. S., Lee, S., Niculescu-Duvaz, D., Good, V. M., Jones, M. C., Marshall, C. J., Springer, C. J., Barford, D., and Marais, R. (2004) Mechanism of activation of the RAF-ERK signaling pathway by oncogenic mutations of B-RAF. *Cell 116*, 855–867.
7. Buchdunger, E., Cioffi, C. L., Law, N., Stover, D., Ohno-Jones, S., Druker, B. J., and Lydon, N. B. (2000) Abl protein-tyrosine kinase inhibitor STI571 inhibits in vitro signal transduction mediated by c-Kit and platelet-derived growth factor receptors. *J. Pharmacol. Exp. Ther. 295*, 139–145.
8. Seeliger, M. A., Nagar, B., Frank, F., Cao, X., Henderson, M. N., and Kuriyan, J. (2007) c-Src binds to the cancer drug imatinib with an inactive Abl/c-Kit conformation and a distributed thermodynamic penalty. *Structure 15*, 299–311.
9. Deininger, M., Buchdunger, E., and Druker, B. J. (2005) The development of imatinib as a therapeutic agent for chronic myeloid leukemia. *Blood 105*, 2640–2653.
10. Atwell, S., Adams, J. M., Badger, J., Buchanan, M. D., Feil, I. K., Froning, K. J., Gao, X., Hendle, J., Keegan, K., and Leon, B. C. (2004) A novel mode of Gleevec binding is revealed by the structure of spleen tyrosine kinase. *J. Biol. Chem. 279*, 55827–55832.
11. Karaman, M. W., Herrgard, S., Treiber, D. K., Gallant, P., Atteridge, C. E., Campbell, B. T., Chan, K. W., Ciceri, P., Davis, M. I., Edeen, P. T., Faraoni, R., Floyd, M., Hunt, J. P., Lockhart, D. J., Milanov,

Z. V., Morrison, M. J., Pallares, G., Patel, H. K., Pritchard, S., Wodicka, L. M., and Zarrinkar, P. P. (2008) A quantitative analysis of kinase inhibitor selectivity. *Nat. Biotechnol. 26*, 127–132.
12. Wilhelm, S., Carter, C., Lynch, M., Lowinger, T., Dumas, J., Smith, R. A., Schwartz, B., Simantov, R., and Kelley, S. (2006) Discovery and development of sorafenib: A multikinase inhibitor for treating cancer. *Nat. Rev. Drug Discovery 5*, 835–844.
13. Simard, J. R., Getlik, M., Grutter, C., Pawar, V., Wulfert, S., Rabiller, M., and Rauh, D. (2009) Development of a fluorescent-tagged kinase assay system for the detection and characterization of allosteric kinase inhibitors. *J. Am. Chem. Soc. 131*, 13286–13296.
14. Kumar, S., Boeh, J., and Lee, J. C. (2003) p38 MAP kinases: Key sgnalling molecules as therapeutic targets for inflammatory diseases. *Nat. Rev. Drug Discovery 2*, 717–726.
15. Wang, Z., Harkins, P. C., Ulevitch, R. J., Han, J., Cobb, M. H., and Goldsmith, E. J. (1997) The structure of mitogen-activated protein kinase p38 at 2.1-Å resolution. *Proc. Natl. Acad. Sci. U.S.A. 94*, 2327–2332.
16. Bellon, S., Fitzgibbon, M. F., Fox, T., Hsun-Mei, H., and Wilson, K. P. (1999) The structure of phosphorylated P38γ is monomeric and reveals a conserved activation-loop conformation. *Structure 7*, 1057–1065.
17. Goldstein, D. M., and Gabriel, T. (2005) Pathway to the clinic: Inhibition of P38 MAP kinase. *Curr. Top. Med. Chem. 5*, 1017–1029.
18. Peifer, C., Wagner, G., and Lauferi, S. (2006) New Approaches to the Treatment of Inflammatory Disorders: Small Molecule Inhibitors of p38 MAP Kinase. *Curr. Top. Med. Chem. 6*, 113–149.
19. Gill, A. L., Frederickson, M., Cleasby, A., Woodhead, S. J., Carr, M. G., Woodhead, A. J., Walker, M. T., Congreve, M. S., Devine, L. A., Tisi, D., O'Reilly, M., Seavers, L. C., Davis, D. J., Curry, J., Anthony, R., Padova, A., Murray, C. W., Carr, R. A., and Jhoti, H. (2005) Identification of novel p38α MAP kinase inhibitors using fragment-based lead generation. *J. Med. Chem. 48*, 414–426.
20. Pargellis, C., Tong, L., Churchill, L., Cirillo, P. F., Gilmore, T., Graham, A. G., Grob, P. M., Hickey, E. R., Moss, N., Pav, S., and Regan, J. (2002) Inhibition of p38 MAP kinase by utilizing a novel allosteric binding site. *Nat. Struct. Biol. 9*, 268–272.
21. Regan, J., Breitfelder, S., Cirillo, P., Gilmore, T., Graham, A. G., Hickey, E., Klaus, B., Madwed, J., Moriak, M., Moss, N., Pargellis, C., Pav, S., Proto, A., Swinamer, A., Tong, L., and Torcellini, C. (2002) Pyrazole urea-based inhibitors of p38 MAP kinase: From lead compound to clinical candidate. *J. Med. Chem. 45*, 2994–3008.
22. Bukhtiyarova, M., Karpusas, M., Northrop, K., Namboodiri, H. V., and Springman, E. B. (2007) Mutagenesis of p38α MAP kinase establishes key roles of Phe169 in function and structural dynamics and reveals a novel DFG-OUT state. *Biochemistry 46*, 5687–5696.
23. Casper, D., Bukhtiyarova, M., and Springman, E. B. (2004) A Biacore biosensor method for detailed kinetic binding analysis of small molecule inhibitors of p38α mitogen-activated protein kinase. *Anal. Biochem. 325*, 126–136.
24. Michelotti, E. L., Moffett, K. K., Nguyen, D., Kelly, M. J., Shetty, R., Chai, X., Northrop, K., Namboodiri, V., Campbell, B., Flynn, G. A., Fujimoto, T., Hollinger, F. P., Bukhtiyarova, M., Springman, E. B., and Karpusas, M. (2005) Two classes of p38α MAP kinase inhibitors having a common diphenylether core but exhibiting divergent binding modes. *Bioorg. Med. Chem. Lett. 15*, 5274–5279.
25. Otwinowski, Z., and Minor, W. (1997) Processing of X-ray diffraction data collected in oscillation mode. *Methods Enzymol. 276*, 307–326.
26. Vagin, A., and Teplyakov, A. (2000) An approach to multi-copy search in molecular replacement. *Acta Crystallogr. D30*, 1622–1624.
27. Murshudov, G. N., Vagin, A., and Dodson, E. J. (1997) *Acta Crystallogr. D53*, 240–255.
28. Emsley, P., and Cowtan, K. (2004) Coot: Model-building tools for molecular graphics. *Acta Crystallogr. D60*, 2126–2132.
29. Han, S., Mistry, A., Chang, J. S., Cunningham, D., Griffor, M., Bonnette, P. C., Wang, H., Chrunyk, B. A., Aspnes, G. E., Walker, D. P., Brosius, A. D., and Buckbinder, L. (2009) Structural characterization of proline-rich tyrosine kinase 2 (PYK2) reveals a unique (DFG-out) conformation and enables inhibitor design. *J. Biol. Chem. 284*, 13193–13201.
30. Mol, C. D., Dougan, D. R., Schneider, T. R., Skene, R. J., Kraus, M. L., Scheibe, D. N., Snell, G. P., Zou, H., Sang, B. C., and Wilson, K. P. (2004) Structural basis for the autoinhibition and STI-571 inhibition of c-Kit tyrosine kinase. *J. Biol. Chem. 279*, 31655–31663.
31. Clark, A. M., Labute, P., and Santavy, M. (2006) 2D Structure Depiction. *J. Chem. Inf. Model. 46*, 1107–1123.
32. Meyer, E. A., Castellano, R. K., and Diederich, F. (2003) Interactions with Aromatic Rings in Chemical and Biological Recognition. *Angew. Chem., Int. Ed. 42*, 1210–1250.
33. Manning, G., Whyte, D. B., Martinez, R., Hunter, T., and Sudarsanam, S. (2002) The protein kinase complement of the human genome. *Science 298*, 1912–1934.
34. Graczyk, P. P. (2007) Gini Coefficient: A New Way To Express Selectivity of Kinase Inhibitors against a Family of Kinases. *J. Med. Chem. 50*, 5773–5779.